Journal of Nuclear Materials 395 (2009) 131–139

Contents lists available at ScienceDirect

Journal of Nuclear Materials

journal homepage: www.elsevier.com/locate/jnucmat

Molecular dynamics simulation of helium and oxygen diffusion in $UO_{2\pm x}$

K. Govers [a,b,*], S. Lemehov [b], M. Hou [c], M. Verwerft [b]

[a] Service de Métrologie Nucléaire (CP 165/84), Université Libre de Bruxelles, 50 av. F.D. Roosevelt, B-1050 Bruxelles, Belgium
[b] Institute for Nuclear Materials Sciences, SCK•CEN, Boeretang 200, B-2400 Mol, Belgium
[c] Physique des Solides Irradiés et des Nanostructures (CP 234), Université Libre de Bruxelles, Bd du Triomphe, B-1050 Bruxelles, Belgium

ARTICLE INFO

Article history:
Received 5 June 2008
Accepted 6 October 2009

PACS:
31.15.Qg
34.20.Cf
61.72.−y
61.72.Ji
66.30.Hs
71.15.Pd
83.10.Rp

ABSTRACT

Atomic scale simulation techniques based on empirical potentials have been considered in the present work to get insight on helium diffusion in uranium dioxide. By varying the stoichiometry, together with the system temperature, the performed molecular dynamics simulations indicate two diffusion regimes for He. The first one presents a low activation energy (0.5 eV) and suggests oxygen vacancies assisted migration. This regime seems to provide the major contribution to diffusion when structural defects are present (extrinsic defects, imposed, e.g. by the stoichiometry). The second regime presents a higher activation energy, around 2 eV, and dominates in the higher temperature range or at perfect stoichiometry, suggesting an intrinsic migration process. Considering the dependance of He behaviour with oxygen defects, oxygen diffusion has been considered as well in the different stoichiometry domains. Finally, further investigations were made with nudged elastic bands calculations for a better interpretation of the operating migration mechanisms, both for He and O.

1. Introduction

The behaviour of noble gases in nuclear fuel, and particularly their release into the rod free volume, is one of the most limiting processes with respect to the fuel performance. The total quantity of produced He remains generally low as compared to the amount of produced fission gas, and moreover the total He balance is often negative (more He is absorbed form the filling gas in the fuel than vice versa), therefore most studies have focused on Xe and Kr [1,2].

In view of this, He release is commonly not modelled in fuel performance codes, or it is assumed to behave in the same way as Xe, with a diffusion coefficient higher by a few orders of magnitude to take into account a supposed higher mobility [2]. However, the relevance of He behaviour in nuclear fuels regains interest in the context of its production by α-emitters in storage conditions and, in-pile, in actinide-containing fuels (MOX and inert matrix fuels), in view of new experiments [3–8] and theoretical studies [9–11] that have been published in the recent years.

In the present work, He diffusion has been investigated by computer simulations, using semi-empirical interatomic potentials. Expressions for He diffusion in different stoichiometry regimes were derived. The results suggest that two migration mechanisms could be operative. It was found that in hypo-stoichiometric fuel (UO_{2-x}), He migration operates via an oxygen vacancy-assisted mechanism which has a low activation energy. In stoichiometric (UO_2) and hyperstoichiometric fuel (UO_{2+x}), He migration operates via direct jumps between interstitial sites and this mechanism has a much higher activation energy. This second mechanism dominates in all cases at elevated temperatures.

These simulations provided at the same time an opportunity to calculate the oxygen diffusion coefficient for the same departures from stoichiometry. Such results are still rather scarce and mainly concern oxygen diffusion in a stoichiometric matrix above 2000 K [12–17]. Very recently, two publications became available about oxygen diffusion in non-stoichiometric uranium dioxide [18,19].

The calculation techniques will be described in Section 2, the results of molecular dynamics simulations will be presented in Section 3 and further interpretations of them will be discussed in Section 4.

2. Calculation method

2.1. Generalities

Computer simulations have been considered to investigate He atomic diffusion in uranium dioxide, where classical semi-empirical interatomic potentials have been used to describe atom interactions. Three techniques based on these potentials have been envisaged:

* Corresponding author. Address: Service de Métrologie Nucléaire (CP 165/84), Université Libre de Bruxelles, 50 av. F.D. Roosevelt, B-1050 Bruxelles, Belgium. Tel.: +32 473413032.
E-mail address: kgovers@sckcen.be (K. Govers).

0022-3115/$ - see front matter © 2009 Elsevier B.V. All rights reserved.
doi:10.1016/j.jnucmat.2009.10.043

- Molecular dynamics techniques, in which one follows the time-evolution of the system. Forces acting on all atoms are calculated at regular intervals from the interatomic potential in order to determine their trajectories.
- Nudged elastic band (NEB) calculations, which simultaneously energy-minimize a set of intermediate configurations in order to find the migration pathway between two atomic configurations.
- Energy minimization, in which atom positions are relaxed until an energy minimum is found. Constraints can be added to the minimization, fixing, e.g. one or more coordinates of an atom. They are used as complement to NEB calculations, in order to better visualize the energy surface during migration.

The last two techniques have been used in order to interpret the migration mechanisms operating during the MD runs.

2.2. Interatomic potential selection

Based on a previous study [20,21], two sets of interatomic potentials describing atomic interactions in the host matrix have been selected: Morelon potential [13] and Basak potential [15]. The detailed description and parametrization of these two potentials can be found in [20,13,15]. These sets of potentials showed a good agreement with experiment on defect properties [20] (formation and migration energies) and thermal properties [21] (lattice expansion, melting temperature), which are essential in view of the calculations we present here.

The interactions involving He atoms (He–O, He–U, He–He) were taken from the work of Grimes et al. [22] and were coupled to both above-mentioned potentials that described the UO_2 matrix. He-host atoms are based on a Lennard–Jones description:

$$V_{ij}(r) = \frac{B_{ij}}{r^{12}} - \frac{C_{ij}}{r^6} \quad (1)$$

The parametrization of these interactions is provided in Table 1. He atoms, described by a shell-core model in [22], were treated in the present work using the commonly-named rigid ions model (for helium, the words "rigid atom model" would be even more appropriate) in view of their low polarisability [11,22].

The Lennard–Jones potential proposed by Grimes et al. [22] has been used in the present work for He–He interactions, even though other elaborated potentials exist [23]. This choice has little influence on the derived results in view of the low He concentration considered (no bubbles were formed), it has the only objective that two He atoms could not share a common site.

The transfer of the He–O, He–U, He–He interactions developed by Grimes et al. [22] to the set of interatomic potentials for UO_2 developed by Morelon et al. [13] and Basak et al. [15] was assessed by recalculating the different incorporation energies. The comparison is reported in Table 2, together with a comparison to ab initio results.

2.3. Molecular dynamics simulations

A conceptually simple method to determine the diffusion coefficient is to compute atom trajectories by molecular dynamics techniques. These techniques have the advantage that no hypothesis is made about the migration path, the system "finds" it by construction. However, in order to have sufficient statistics over a run, a significant number of atomic jumps is needed. Therefore only processes with a relatively low activation energy can be simulated within a reasonable amount of time.

The diffusion coefficient of solute atoms in a matrix (or a solvent) can be estimated using the Einstein relation between D and the mean square displacement $< |\boldsymbol{r}(t) - \boldsymbol{r}(0)|^2 >$:

$$< |\boldsymbol{r}(t) - \boldsymbol{r}(0)|^2 >= \mathrm{MSQD} + 6Dt \quad (2)$$

This equation is valid for $t \to \infty$. The mean square quadratic displacement (MSQD) represents the spread of the ion motion around their equilibrium position, and the second term comes from diffusion itself. MSD curves have been fitted to Eq. (2) to derive the diffusion coefficient for each MD simulation performed. The mean square displacement is derived from the system trajectory. Considering N particles of one species, it is given by:

$$< |\boldsymbol{r}(t) - \boldsymbol{r}(0)|>^2 = \frac{1}{NN_t} \sum_{n=1}^{N} \sum_{t_0}^{N_t} |r_n(t+t_0) - r_n(t_0)|^2 \quad (3)$$

where $r_n(t)$ is the position of the nth particle at time t. The sum over different t_0 (N_t terms) enables for better statistics.

The MD runs were performed with a system containing $12 \times 12 \times 12$ conventional unit cells (total of 20,736 ions), and 104 He atoms randomly distributed, initially in octahedral position. Such a large system was needed in order to improve the statistics, averaging the mean square displacements of a larger amount of atoms. The system was first brought to the desired temperature initializing the velocities from a Maxwell–Boltzmann distribution and applying a re-scaling procedure (every 0.05 ps) for 1 ps. The system pressure was kept close to zero by an adequate choice of the system volume, based on our previous study [21]. The remaining of the simulation was run in the NVE ensemble. Atom positions were extracted every 0.1 ps during 25 ps, after an additional equilibration period of 4 ps. Illustrations of mean square displacement curves are shown in Fig. 1a and b. The diffusion coefficient was then calculated by a least square fitting of the slope of the mean square displacement evolution with time.

By computing the diffusion coefficient at different temperatures (from 1000 to 3000 K by steps of 250 K), one can fit the results to an Arrhenius form. In addition to a non-defective host matrix, different departures from stoichiometry were simulated by modifying the concentration of oxygen point defects (vacancies or interstitial): 0%, 0.5%, 1%, 2% and 5%, covering the stoichiometry range

Table 1
He–O, He–U, He–He interactions [22]: Lennard–Jones type, Eq. (1).

	B_{ij} (eV Å^{12})	C_{ij} (eV Å^6)
He–He	69.3559	0.493712
He–O	2247.836	11.762
He–U	500.425	7.366

Table 2
Energy (in eV) of He incorporation energies as obtained with the potentials used in the present work, Grimes' original potential [22] and ab initio results of Freyss et al. [9]. Energies at different locations were considered (their identification in the $Fm\bar{3}m$ space group is provided between brackets): in octahedral interstitial position (IOP, 4*b* site), at the mid-point between two of these octahedral interstitial positions (24*d* site), in an V_O site (8*c* site), at the mid-point between an $V_O^{\cdot\cdot}$ location and an octahedral interstitial position (32*f* site, with $x,y,z = 0.375$), and at a $V_U^{''''}$ location (4*a* site). For mid-point calculations, constrained energy minimization was used for He atom coordinates.

	Basak	Morelon	Grimes Re-calc.	Grimes Or. val.	Freyss Ab initio
He location					
4*b* (in IOP)	−0.1	−0.1	−0.1	−0.11	−0.1
24*d*	4.1	2.6	4.2	3.8	
8*c* (in $V_O^{\cdot\cdot}$)	−0.09	−0.19	−0.23	−0.19	2.4
32*f*, $x,y,z = 0.375$	0.47	0.37	0.44	0.38	
4*a* (in $V_U^{''''}$)	−0.2	0.18	−0.2	−0.19	0.4

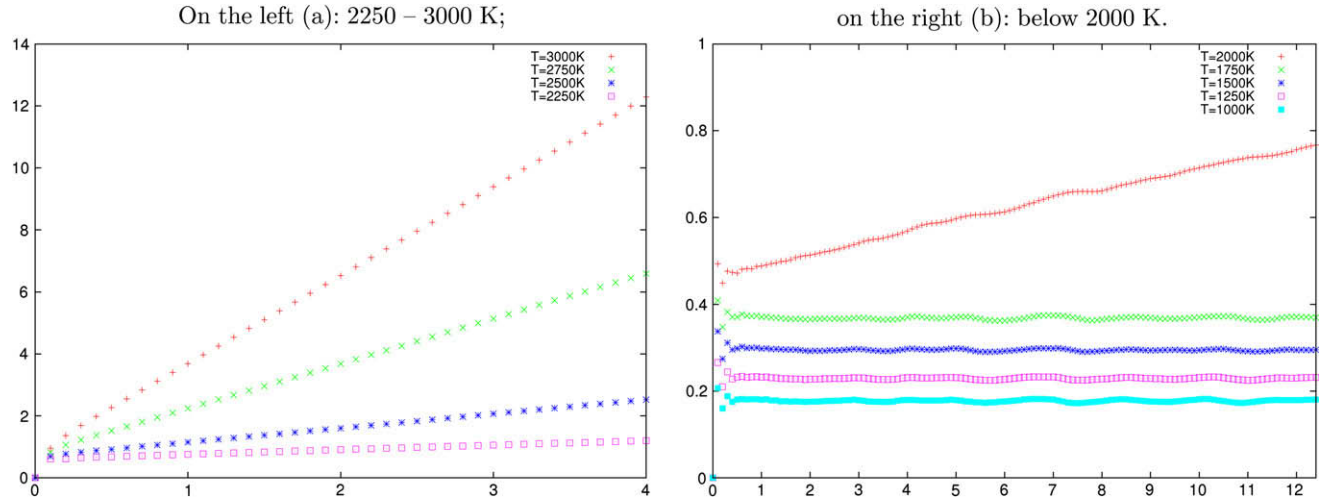

Fig. 1. Evolution with temperature of oxygen mean square displacement curve in perfectly stoichiometric UO_2. On the left (a): 2250–3000 K and on the right (b): below 2000 K.

from $UO_{1.90}$ to $UO_{2.10}$; point defects positions were chosen at random.

2.4. Nudged Elastic Bands calculations

"Nudged Elastic Bands" (NEB) calculations allow to find the optimum migration pathway between two different atomic configurations. Their implementation in DL_POLY [24] works a follow:

- Determine two energy-minimized configurations between which the optimum migration pathway is to be searched.
- Generate intermediate states by linear interpolation between both initial configurations, these intermediate states are called the "beads" of the NEB "chain".
- The beads are connected with each other by a harmonic spring, with a user-defined force constant.
- The system energy of the whole chain, including the energy of the successive springs, is minimized with the atomic coordinates in the intermediate beads as degrees of freedom. The springs impede the relaxation of an intermediate bead into the nearest local minimum.
- Refinement is brought ("nudging") to this simple description, by ensuring that the forces acting on the beads are approximately orthogonal to the forces optimizing the bead configuration. It should provide evenly spaced beads along the migration path. The maximum energy along the chain corresponds then to the migration energy between both initial structures.

The migration energy is an important parameter in the expression of the diffusion coefficient; however, energy minimization cannot be used to fully characterize the diffusion coefficient because the dynamic part (i.e. jump attempt frequency) is not modelled. It is therefore often coupled to molecular dynamics simulations: as a complementary technique, to derive migration energies and pathways, or in order to use these quantities in hyperdynamics simulations, like Temperature Accelerated Dynamics [24].

2.5. Constrained energy minimization

Energy minimization involves finding a configuration that minimizes the system energy, starting from a chosen atomic configuration. Constraints can be added to the minimization ("constrained energy minimization", CEB), e.g. by keeping an atom's x, y, and/or z coordinate (or any combination of them) fixed. The defect energy calculation was based on the Mott–Littleton method, implemented in the GULP [25] code. It considers a full relaxation for atoms inside a first sphere and an approximate relaxation for atoms at larger distance form the defect, until a second sphere beyond which a continuous dielectric medium is assumed. Sphere radii of, respectively, 9 and 20 Å were shown earlier [20] to provide a good energy convergence. This technique has been used as a complement to NEB calculations in order to better vizualize the migration pathways and barriers. A constrained relaxation was applied to the system, where the x- and y-coordinates of the migrating He atom were fixed at each step, the relaxation being allowed in the z-direction and for all other atoms. By repeating such calculation at different x and y values, the energy surface the migrating atom is subjected to during its migration could be sampled. In the present work, the relaxed configuration for a He atom at a location (x_0, y_0) was us ed as basis for the relaxation at the location $(x_0 + \Delta x, y_0)$, and an identical procedure was used to start a new "line" in the y-direction. Δx and Δy intervals were set to 0.03 Å.

3. Diffusion coefficient analysis (MD simulations)

3.1. Helium diffusion in $UO_{2\pm x}$

MD simulations of He in UO_2 were made at temperatures ranging from 1000 to 3000 K, by steps of 250 K. Various departures from stoichiometry were in each case considered in order to derive an Arrhénius expression for He diffusion in the different stoichiometry domains. The departure from stoichiometry was modelled by creating randomly dispersed oxygen point defects: vacancies and interstitials for respectively the hypo- and hyperstoichiometric regions. The influence of uranium defects has been qualitatively assessed by performing a separate effect study. Their influence on helium diffusion is discussed in Section 3.3.

He diffusion coefficient as derived from the MD runs are plotted in Figs. 2 and 3 (respectively the hypo- and hyperstoichiometry domains) for both Morelon and Basak potentials.

It clearly appears on these graphs that He diffusion at low temperatures is assisted by oxygen vacancies, and presents a very low activation energy, around 0.5 eV (see Fig. 2). In the high temperature region, as well as for stoichiometric and hyperstoichiometric

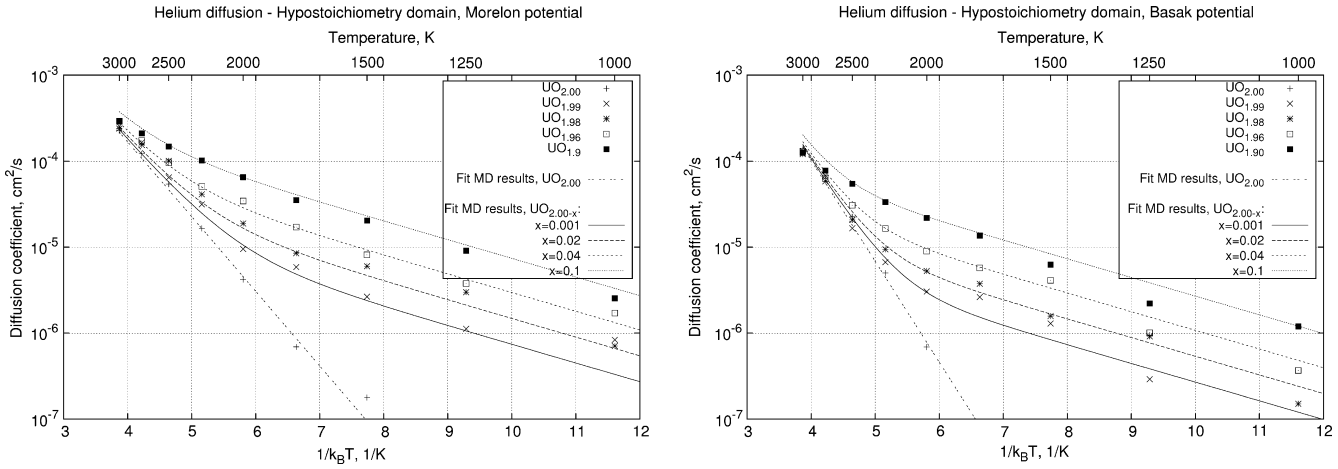

Fig. 2. He diffusion coefficient in the hypostoichiometry domain. Left: Morelon and right: Basak potentials.

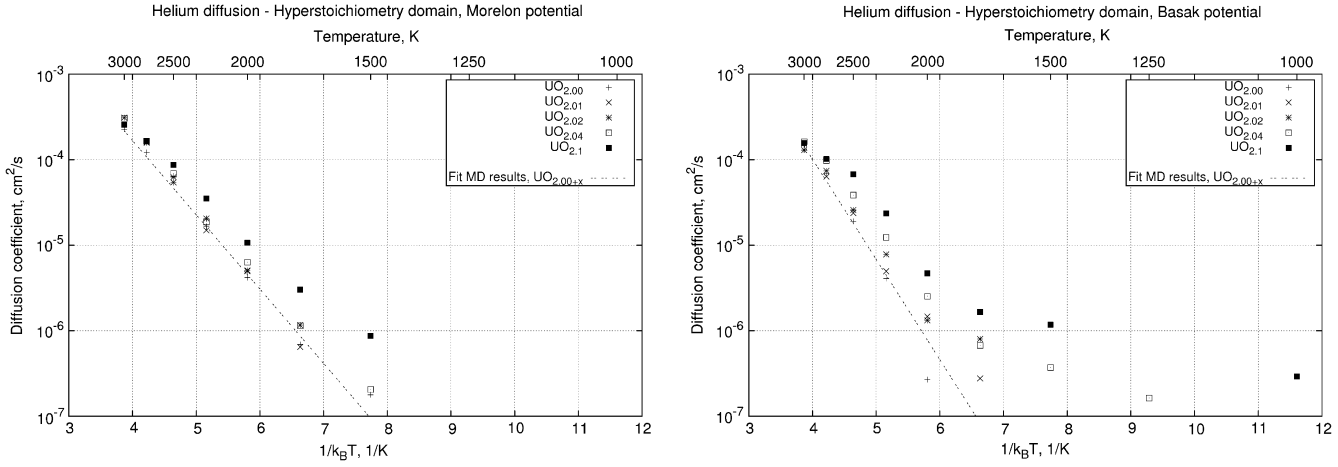

Fig. 3. He diffusion coefficient in the hyperstoichiometry domain. Left: Morelon and right: Basak potentials.

uranium dioxide, the activation energy presents a higher value, around 2.1 eV. Such a behaviour could be expected since at high temperature, or in absence of structural defects, thermally generated defects dominate whose concentration shows a Boltzmann dependance on both the temperature and the formation energy of the defect. In that case, the activation energy is given by the sum of the migration energy and the formation energy of the assisting defect.

Considering that the vacancy formation energy at stoichiometry is given by half the formation energy of an oxygen Frenkel pair (E_{OFP}), with a value of approximately $\frac{1}{2} \times 3.2$–$4.6\ \text{eV} = 1.5$–$2.3\ \text{eV}$ [20], a value in the 2–3 eV range could easily be explained assuming V_O-assisted migration is still operating. However, in that case, a still larger activation energy should be observed in the hyper-stoichiometric domain (since the formation energy of a vacancy in UO_{2+x} amounts to E_{OFP}), which is not the case. Therefore, the 2.1 eV activation energy should correspond to a second, intrinsic, migration mechanism. Further insights on the migration mechanism will be given in the next section, thanks to NEB and static calculations.

The expression that we could derive for He intrinsic diffusion coefficient, i.e. in the stoichiometric and hyperstoichiometric domain, is the following:

$$D_{\text{He,int}} = 0.5 \exp\left(\frac{-2.0\ \text{eV}}{k_B T}\right) \text{cm}^2/\text{s} \tag{4}$$

and for the V_O-assisted mechanism, with x the departure from stoichiometry:

$$D_{\text{He},V_O} = 0.011 \cdot x \cdot \exp\left(\frac{-0.5\ \text{eV}}{k_B T}\right) \text{cm}^2/\text{s} \tag{5}$$

3.2. Oxygen diffusion in $UO_{2\pm x}$

In view of the importance of oxygen defects for He migration in $UO_{2\pm x}$, some attention has also been paid to oxygen self-diffusion in the different stoichiometry domains. Such MD results for oxygen diffusion in UO_2 are still poorly covered in the open literature, with a few works devoted to perfectly stoichiometric UO_2 [12–16], in a nano-crystal (small system with free surfaces) [17], and recently in hypo-stoichiometric [18] and hyper-stoichiometric [19] uranium dioxide.

The diffusion coefficients derived from the MD runs with Basak and Morelon potentials at different temperatures are plotted in Figs. 4 and 5 for, respectively, the hypo- and hyper-stoichiometry regions. A fitting of these points to an Arrhénius expression as a function of the stoichiometry departure is provided in Table 5, together with comparison to other MD, ab initio and experimental results. A good agreement is observed on both the prefactor D_0 and the activation energy E_{act} in UO_{2-x} and $UO_{2.00}$. It can be observed that the calculations with Basak potential (much less so for the Morelon potential) show that for highly hypostoichiometric UO_{2-x} ($x > 0.1$), the activation energy is increased, probably due to

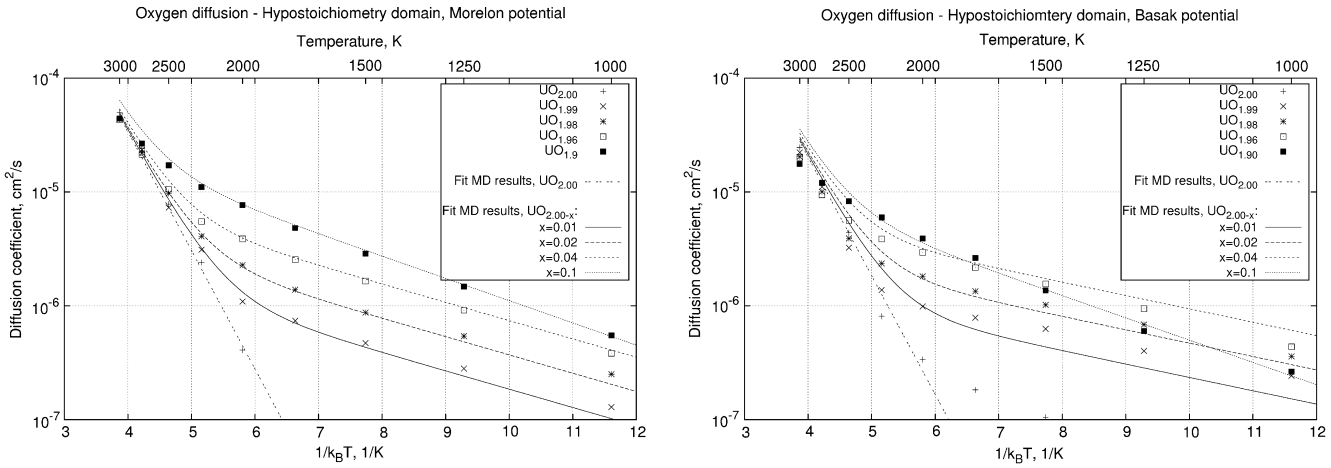

Fig. 4. O diffusion coefficient in the hypostoichiometry domain. Left: Morelon and right: Basak potentials.

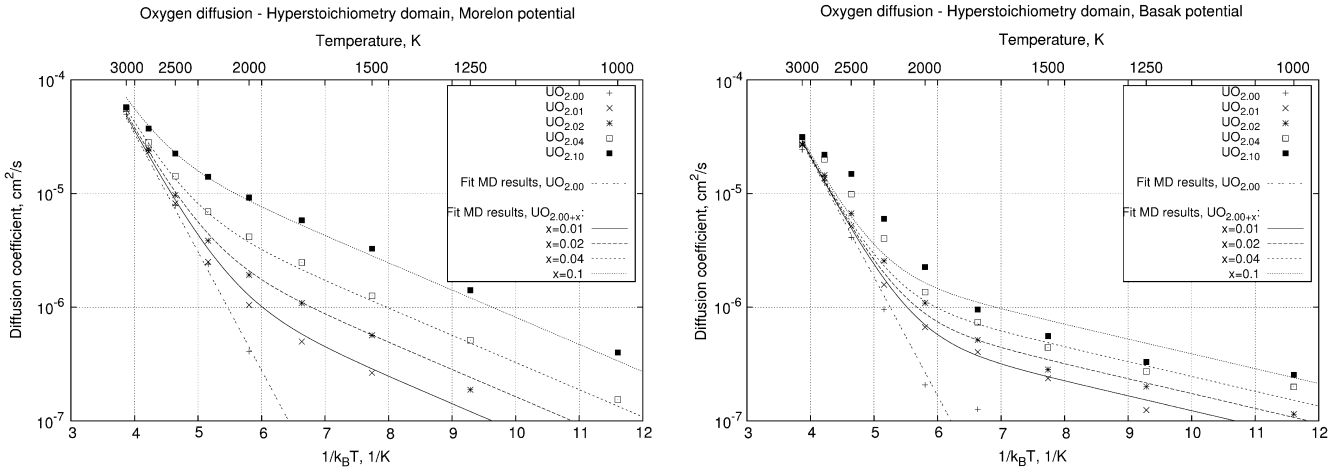

Fig. 5. O diffusion coefficient in the hyperstoichiometry domain. Left: Morelon and right: Basak potentials.

the large concentration of vacancies and to interactions starting between them. The predicted behaviour in the hyperstoichiometry region is far different for both potentials. Morelon potential predicts an activation energy half of that observed experimentally; while Basak potential predicts a still lower activation energy. Further detail about the operating migration mechanisms in the different stoichiometry domains will be provided in the next section.

In stoichiometric fuel, or at high temperature, oxygen diffusion coefficient presents an activation energy of 2.4 eV (see Table 5 and Figs. 4 and 5). Yakub et al. [16] associate a change of slope in the vicinity of 2000–2500 K, with a λ-transition. Contrary to their work, such a change could not be observed in our estimation of oxygen diffusion coefficient between 2000 and 3000 K. Lower temperature results were not exploited for diffusion at stoichiometry because of the too large uncertainties on diffusion coefficient values below 10^{-7} cm^2/s that are derived from MSD curve (limited due to the system size and simulation times considered in the present work). Indeed, in such conditions, the slope of the MSD was concealed by the fluctuations of the ions mean quadratic displacement around their equilibrium position (this is illustrated in Fig. 1). Changes associated to a λ-transition below 2000 K should therefore be investigated with larger systems and/or for longer simulation times. In view of the system sizes (20,736 compared to 324–12,000 atoms) and simulation times (25 ps compared to 10–40 ps) used in both works, similar uncertainties on the results should prevail, and the possible influence of the λ-transition in that temperature region be considered with caution.

3.3. He trapping on uranium vacancies

Even though enhancement of He diffusion is not expected in presence of uranium vacancies (considering their lower mobility, with a migration energy above 2 eV [20], such defects could influence He mobility through a trapping effect. A MD study similar to those of Section 3 was therefore performed, only with Morelon potential, this time considering uranium instead of oxygen vacancies. When He atoms were initially located into octahedral interstitial sites, no effect of uranium vacancies could be observed on the diffusion coefficient. However, when He atoms were initially located *at* uranium vacancy sites, the diffusion coefficient decreased by three orders of magnitude (see Fig. 6). These observation show the trapping effect of uranium vacancies on He atoms, and could explain the large difference observed for the prefactor of He diffusion derived here and that determined experimentally.

Similarly, when uranium *and* oxygen defects were inserted, only trapping effects could be observed, without modification to the activation energy. This observation was made for both randomly distributed uranium and oxygen vacancies, as well as for randomly distributed trivacancies (close configuration of a uranium and two oxygen vacancies).

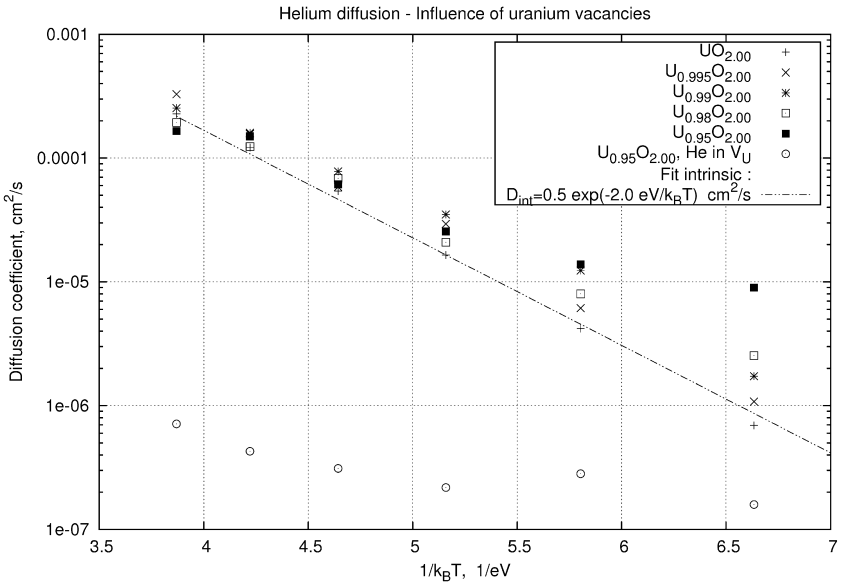

Fig. 6. He diffusion coefficient in presence of randomly distributed uranium vacancies.

4. Migration path analysis (NEB and CEM calculations)

4.1. Helium migration

To further elucidate the mechanism of He diffusion and to study the diffusion path in more detail, NEB calculations were performed. Such calculations are commonly coupled to molecular dynamics simulations in order to get insight on the migration mechanism or to accelerate the computed dynamics of the system like in Temperature Accelerated Dynamics simulations [24,26]. In a first time He diffusion was considered, both in a perfect lattice and in presence of one oxygen vacancy. Then, considering the importance of oxygen defects, specific calculations were also made for oxygen migration.

To that aim, we started Temperature Accelerated Dynamics (TAD) calculations, as implemented in the DL_POLY 2.19 software [24], considering a system consisting of $4 \times 4 \times 4$ UO_2 conventional unit cells (256 U and 512 O atoms), where a He atom was inserted as well, in one of the octahedral interstitial positions (4*b* site in a $Fm\bar{3}m$ space group). This technique was used to explore, for the He atom, the different escape pathways from the interstitial position it was initially located in. A jump was recorded if an atom, after energy-minimization of the system configuration, was displaced by more than 1 Å. For each computed jump, a NEB calculation was then initiated between the original and the final configurations. Once a jump has occured, the configuration returns to the original one and the simulation proceeds again, in order to explore other possible migration pathways. The TAD simulations performed ran for 500 ps at 2000 K, with an energy minimization (to detect transitions) every 0.05 ps.

The NEB calculations showed a very good agreement with the migration energies derived from the MD runs, providing in addition the migration pathway. The calculated migration energies are reported in Table 3, together with MD and experimental migration energies. A similar procedure has been considered to derive the migration energy in presence of an oxygen vacancy. These results are reported in Table 3. Concerning the migration pathway, the results show a migration from an octahedral interstitial site to an equivalent one when no V_O is present, and a migration to the vacant oxygen site when an V_O is in an adjacent place. Considering the small energy difference between both site locations (less than 0.1 eV), a similar migration energy applies to jump back from the V_O site to the interstitial site. In Figs. 7 and 8, the migration mechanism is illustrated. These results were derived from a large series of energy minimization calculations, mapping the (x, y) coordination plane with a fine mesh, and in each individual calculation, the *x*- and *y*-coordinates of the He atom were kept fixed. The migration energies calculated that way are in excellent agreement with the NEB calculations, but are approximately 1000 times longer to be performed.

Table 3
He migration energies between two octahedral interstitial positions (OIS) and between an interstitial position and an oxygen vacancy, NEB calculations with Basak and Morelon potentials.

	Basak (eV)	Morelon (eV)
Migration mechanism		
$He_{OIS} \rightarrow He_{OIS}$	3.5	2.26
$He_{OIS} \rightarrow He_{V_O}$	0.42	0.42–0.48

The next TAD step usually consists of extrapolating the system evolution at high temperature to a lower temperature. The repetition of such step was not needed here, as the different diffusion pathways could be identified and enough statistics to derive the diffusion coefficient were already obtained from the MD runs of Section 3.

4.2. Oxygen migration

Oxygen migration has been assessed as well with TAD/NEB calculations, with a similar methodology as for He migration. Three systems similar to the previous case were considered, except that no He atom was inserted:

- a non-defective $4 \times 4 \times 4$ supercell (768 atoms) to represent the perfect stoichiometry;
- a $4 \times 4 \times 4$ supercell from which one oxygen atom has been removed, to investigate migration of the oxygen vacancy;
- a $4 \times 4 \times 4$ supercell in which one oxygen atom has been added, to investigate migration of an isolated oxygen interstitial.

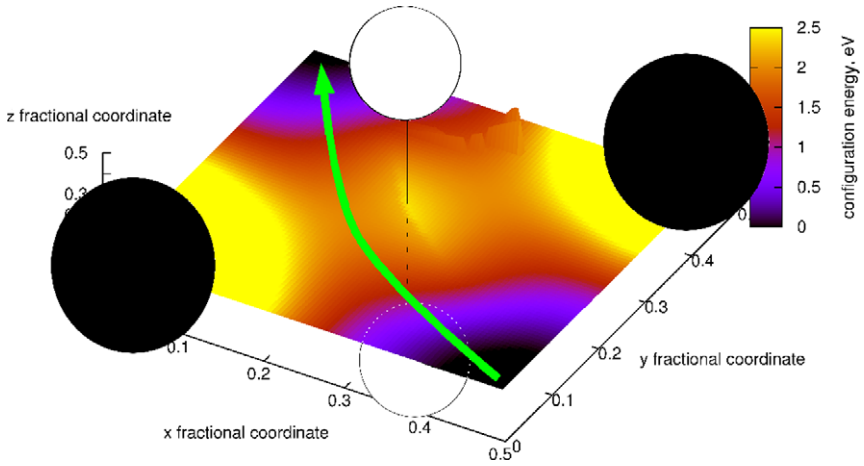

Fig. 7. Determination of He migration pathway in a regular crystal, Morelon potential. The graph shows the relaxed He position in the *z*-direction as a function of its *x*- and *y*-coordinates (fractional coordinates were used), and the color indicates the energy of the configuration, relative to the minimum energy configuration. The energy barrier is about 2.3 eV. The migration pathway is illustrated in green. (For interpretation of the references to colour in this figure legend, the reader is referred to the web version of this article.)

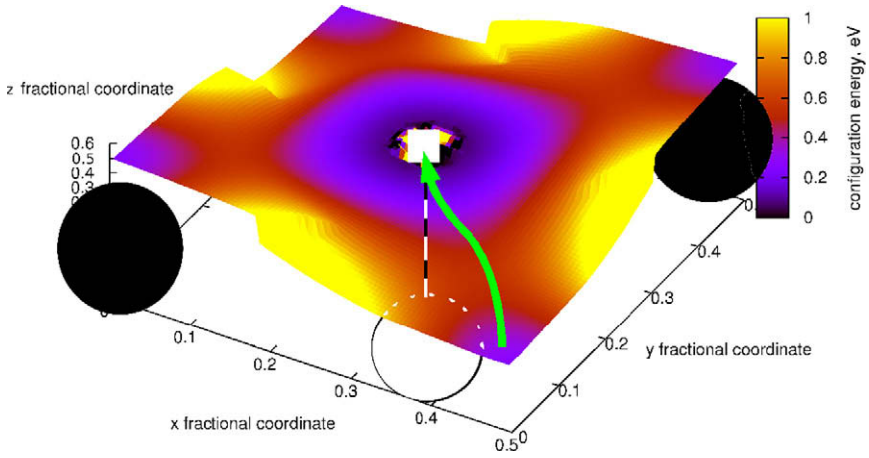

Fig. 8. Determination of He migration pathway for V_O-assisted migration, Morelon potential. The same formalism was used as in the previous figure, but with a different color-scale for the energy. The energy barrier in presence of a vacancy is about 0.5 eV. The migration pathway is illustrated in green. The sudden changes of energy near the oxygen vacancy are due to convergence problems of the energy minimization technique.

The migration energies obtained with this technique are reported in Table 4. No clusters of interstitials were considered in the present NEB calculations in view of the weak influence of oxygen interstitials on He diffusion and considering the work performed by Ichinomiya et al. [18]. The low activation energy derived from the MD runs with Basak potential is in poor agreement with the NEB calculations presented here, but a very good correspondence is found with the results derived by Ichinomiya, also obtained with Basak potential, for cluster migration.

The other migration energies derived here confirmed those obtained in our previous general comparison of interatomic potentials for UO_2 [20,21] for oxygen vacancies and interstitials, as well as other studies with the same potentials [13,15,18].

However, for the stoichiometric compound, the calculations indicate that the major contribution to oxygen diffusion is neither coming from interstitials neither vacancies migration, but rather from an "unexpected mechanism": the simultaneous migration of 4 regular oxygen atoms in a {1 0 0} plane by permutation of their places:

$$O_1 \rightarrow O_2 \rightarrow O_3 \rightarrow O_4 \rightarrow O_1$$

Other events were also recorded, such as the formation of an oxygen Frenkel pair, but with a lower frequency and a much higher formation energy. For Basak potential, another event where 8 atoms permuted their place could be observed, with a higher migration energy (see Table 4).

This observation, if confirmed by other techniques, questions the reliability of Oxygen Frenkel pair formation energies derived from diffusion experiments (e.g. [27,28]), since it is then assumed that oxygen diffusion operates at stoichiometry through the migration of thermally created interstitials or vacancies. In addition, an extension of this mechanism to the permutation of a larger number of atoms, at sufficiently high temperatures, could be another way

Table 4
Oxygen migration energies for different mechanisms, NEB calculations with Basak and Morelon potentials.

Migration pathway	Basak (eV)	Morelon
$V_{\ddot{O}}$ migration	0.22–0.29	0.25–0.32 eV
Single O_i'' migration	0.9	0.53 eV
Permutation of 4 atoms	4.2	3.1–3.27 eV
Permutation of 8 atoms	7.1	Event not observed

Table 5
Comparison of the derived parameters for the diffusion coefficient to other sources (MD results and experimental values). The *x*-dependance column indicates by which function the prefactor of the diffusion coefficient should be multiplied to take into account the diffusion coefficient variation with *x*.

Stoichiometry	UO_{2-x}			UO_2		UO_{2+x}		
Parameter (units)	*x*-dependance (–)	D_0 (cm^2/s)	E_{act} (eV)	D_0 (cm^2/s)	E_{act} (eV)	*x*-dependance (–)	D_0 (cm^2/s)	E_{act} (eV)
Morelon[a]	x	0.00075	0.37	0.5	2.4	x	0.0020	0.55
	$x = 0.1$	0.00100	0.45					
Basak	x	0.00035	0.27	0.3	2.4	$\sqrt{x}$	0.0000	0.3
	$x = 0.1$	0.00045	0.45					
Other MD sources[a]								
Kupryazhkin et al. [17], bulk				0.26–0.8	2.6–2.76			
Kupryazhkin et al. [17], surface				0.01	1.6			
Govers et al. [20]		0.2–0.6						0.6–1.3
Ichinomiya et al. [18]		0.26						0.9 (single O_i)
								0.14–0.24 (clusters)
Ab initio results (*only* E_{mig})								
Gupta et al. [30,31]	1.0–1.2						0.7–1.1	
Experimental results								
Matzke [27,28] (recom.)				0.26	2.55	x	0.0045	0.94
Kim and Olander [32]	x	0.00022	0.5			x	0.0045	0.94
Contamin et al. [33]						x	0.0045	0.94

[a] Only works where an expression for the diffusion coefficient was derived are referred in the table. For Morelon potential, the diffusion coefficient at stoichiometry derived in [13] is similar to the one derived here, it is therefore not been added in the comparison table.

to explain the sudden increase of oxygen mobility observed at the λ-transition in fluorite systems.

5. Discussion

5.1. First interpretation of the MD simulations results

In view of the results of Section 3, two different mechanisms can govern helium diffusion in uranium dioxide. At low temperature and in the hypostoichiometric region, diffusion is assisted by oxygen vacancies. The rate-determining step of this mechanism seems to be the jump of the He atom itself, rather than the motion of oxygen vacancies, in view of their lower migration energy.

The results also indicated a probable second mechanism, that could not be linked to V_O-assisted migration in view of the similar He diffusion curves in the stoichiometric and hyperstoichiometric domains.

5.2. Helium behaviour

Different calculation techniques involving empirical interatomic potentials were used in the present work to investigate the diffusion of helium and its migration mechanism in uranium dioxide and for departures from stoichiometry ranging from −0.1 to 0.1. The simulations predict two migration mechanisms for helium. One of them is active in presence of structural oxygen vacancies and has a low activation energy, around 0.5 eV. NEB calculations have confirmed a vacancy-assisted mechanism, which implies jumps between octahedral interstitial positions and oxygen vacancy locations, and that the observed migration energy corresponds to the barrier between both sites. When there are no extrinsic oxygen vacancies (i.e. in stoichiometric and hyperstoichiometric systems), oxygen vacancies can still be created at elevated temperatures as intrinsic defects. It was, however, found that at elevated temperatures another diffusion mechanism is operative, with direct jumps of He atoms between octahedral sites, with a migration energy around 2.0 eV. This is confirmed by both the MD and the NEB calculations.

Both above-mentioned activation energies were also obtained experimentally [3–5,29], but the experimental prefactor presents a large scatter, which can, according to our observations, be explained in terms of trapping due to uranium vacancies, or possibly intragranular bubbles.

5.3. Oxygen behaviour

Considering the impact of oxygen defects on helium migration, oxygen diffusion has been considered as well in the present study, with the same techniques that were used for helium migration. The use of NEB calculations enabled to better identify the migration mechanism predicted by MD simulations, particularly for what concerns diffusion at stoichiometry. Indeed, for both potentials, the major contribution to diffusion occurs through a simultaneous exchange of position of four (or more) atoms. The permutation occurs through motion of atoms along $<100>$ directions. This observation, if confirmed by other techniques, questions the reliability of Frenkel pair energies derived from diffusion coefficients measurements. The migration energy associated to oxygen vacancies motion was for both potentials in the range 0.2–0.3 eV. This low migration energy confirms that the rate-determining step for He migration is the jumping of He atoms. Less attention has been paid to the hyperstoichiometry region in view of its low influence on He mobility. Only migration of single interstitials was considered with NEB techniques. The disagreement between NEB calculations and MD simulations for the Basak potential shows that another migration mechanism, with a much lower activation energy, is operative, probably involving the migration of clusters of interstitials, as shown by Ref. [18].

The results obtained for oxygen diffusion agree very well with experimental data for stoichiometric uranium dioxide, and with previous work on MD simulations of oxygen diffusion; but the calculations in off-stoichiometric systems predict slightly underestimated migration energies of vacancies and interstitials compared to the experimental values.

6. Conclusion

This work showed how He diffusion can be influenced by the oxygen and uranium defects in UO_2. At low temperature, He diffusion is assisted by extrinsic oxygen vacancies. At high temperature or if no extrinsic oxygen vacancies are present (as is the case in stoichiometric and hyperstoichiometric systems), an intrinsic

diffusion mechanism occurs, by atomic jumps from interstitial to interstitial sites. The role of uranium vacancies is more difficult to quantify, but it appears that they can act as traps for He atoms, and therefore considerably reduce the diffusion coefficient. The activation energy seemed, however, unaffected. Trapping by uranium defects, and possibly by intragranular bubbles, can explain the bad agreement in terms of prefactor and the good agreement on activation energy between the present simulation results and experimental measurements.

We also investigated oxygen diffusion, not only for a stoichiometric fuel, but also for different departures from stoichiometry, at temperatures starting at 1000 K. MD results showed a good agreement with experimental data, reproducing the observed activation energies in all stoichiometry regimes. A quite unexpected migration mechanism could be identified in stoichiometric UO_2, namely a circular permutation of four oxygen atoms located in the same $\{100\}$ plane, the motion of each atom occurring along $<100>$ directions.

Acknowledgments

Part of this work was funded by the Université Libre de Bruxelles (ULB) and the SCK•CEN through a PhD grant. This work also took benefit of a participation to the EFP6 ACTINET network of excellence and the EFP7 F-BRIDGE Project.

References

[1] P. Blanpain et al., Recent results from the in-reactor MOX fuel performance in france and improvement program, in: Proceedings of the International Topical Meeting on Light Water Reactor Fuel Performance, Portland, OR, USA.
[2] M. Lippens, B. Lance, D. Boulanger, Plutonium ageing and MOX fuel performance, in: Proceedings of Global 2005, Paper 023.
[3] D. Roudil, X. Deschanels, P. Trocellier, C. Jégou, S. Peuget, J.-M. Bart, J. Nucl. Mater. 325 (2004) 148.
[4] S. Guilbert, T. Sauvage, P. Garcia, G. Carlot, M.-F. Barthe, P. Desgardin, G. Blondiaux, C. Corbel, J. Piron, J.-M. Gras, J. Nucl. Mater. 327 (2004) 88.
[5] C. Ronchi, J. Hiernaut, J. Nucl. Mater. 325 (2004) 1.
[6] F. Garrido, L. Nowicki, G. Sattonnay, T. Sauvage, L. Thomé, Nucl. Instrum. Meth. Phys. Res. B 219–220 (2004) 196.
[7] T. Sauvage, H. Erramli, S. Guilbert, L. Vincent, M.-F. Barthe, P. Desgardin, G. Blondiaux, C. Corbel, J. Piron, F. Labohm, A. Van Veen, J. Nucl. Mater. 327 (2004) 159.
[8] G. Sattonnay, F. Garrido, L. Thomé, Philos. Mag. Lett. 94 (2) (2004) 109.
[9] M. Freyss, N. Vergnet, T. Petit, J. Nucl. Mater. 352 (2006) 144.
[10] Y. Yun, O. Eriksson, P. Oppeneer, J. Nucl. Mater. 385 (2009) 72.
[11] D. Parfitt, R. Grimes, J. Nucl. Mater. 381 (2008) 216.
[12] P. Lindan, M. Gillan, Philos. Mag. B 69 (1994) 535.
[13] N.-D. Morelon, D. Ghaleb, J.-M. Delhaye, L.V. Brutzel, Philos. Mag. 83 (2003) 1533.
[14] C. Meis, A. Chartier, J. Nucl. Mater. 341 (2005) 25.
[15] C. Basak, A. Sengupta, H. Kamath, J. Alloys Compd. 360 (2003) 210.
[16] E. Yakub, C. Ronchi, D. Staicu, J. Chem. Phys. 127 (2007) 094508.
[17] A. Kupryazhkin, A. Zhiganov, D. Risovany, K. Nekrassov, V. Risovany, V. Golovanov, J. Nucl. Mater. 372 (2008) 233.
[18] T. Ichinomiya, B. Uberuaga, K. Sickafus, Y. Nishiura, M. Itakura, Y. Chen, Y. Kaneta, M. Kinoshita, J. Nucl. Mater. 384 (2009) 315.
[19] E. Yakub, C. Ronchi, D. Staicu, J. Nucl. Mater., in press. doi:10.1016/j.jnucmat.2009.01.029.
[20] K. Govers, S. Lemehov, M. Hou, M. Verwerft, J. Nucl. Mater. 366 (2007) 161.
[21] K. Govers, S. Lemehov, M. Hou, M. Verwerft, J. Nucl. Mater. 378 (2008) 66.
[22] R. Grimes, R. Miller, C. Catlow, J. Nucl. Mater. 172 (1990) 123.
[23] K. Tang, J. Toennies, J. Chem. Phys. 118 (2003) 4976.
[24] W. Smith, Mol. Simulat. 32 (2006) 933.
[25] J. Gale, General Utility Lattice Program, Version 1.3, IVEC. <http://www.ivec.org/gulp/>.
[26] A. Voter, F. Montalenti, T. Germann, Annu. Rev. Mater. Res. 32 (2002) 321.
[27] H. Matzke, J. Chem. Soc. Faraday Trans. 2 (83) (1987) 1121.
[28] H. Matzke, Diffusion Processes in Nuclear Fuels, Elsevier Science Publishers, 1992.
[29] P. Garcia, Private Communication, 2008.
[30] F. Gupta, G. Brillant, A. Pasturel, Philos. Mag. 87 (2007) 2561.
[31] F. Gupta, Etude du comportement du produit de fission césium dans le dioxyde d'uranium par méthode ab initio, Ph.D. Thesis, Université de Paris-XI, 2008.
[32] K. Kim, D. Olander, J. Nucl. Mater. 102 (1981) 192.
[33] P. Contamin, J.J. Bacmann, J. Marin, J. Nucl. Mater. 42 (1972) 54.